AGU PUBLICATIONS

Global Biogeochemical Cycles

RESEARCH ARTICLE
10.1002/2016GB005380

Key Points:
- Profiling floats are used to estimate respiration, export production, and export efficiency in eight geographically distinct regions
- Generally, there is greater respiration and export at high latitude, although float estimates may be biased at low latitude
- Depth-integrated respiration is significantly correlated to surface chlorophyll, net primary production, and planktonic size

Correspondence to:
T. D. Hennon,
thennon@uw.edu

Citation:
Hennon, T. D., S. C. Riser, and S. Mecking (2016), Profiling float-based observations of net respiration beneath the mixed layer, *Global Biogeochem. Cycles*, *30*, 920–932, doi:10.1002/2016GB005380.

Received 27 JAN 2016
Accepted 1 JUN 2016
Accepted article online 8 JUN 2016
Published online 29 JUN 2016

Profiling float-based observations of net respiration beneath the mixed layer

Tyler D. Hennon[1], Stephen C. Riser[1], and Sabine Mecking[2]

[1] School of Oceanography, University of Washington, Seattle, Washington, USA, [2] Applied Physics Laboratory, University of Washington, Seattle, Washington, USA

Abstract We employ profiling floats with dissolved oxygen sensors to observe in situ temporal oxygen evolution below the mixed layer, allowing us to characterize net respiration of organic carbon in eight distinct regions over the globe. Export and export efficiency are generally high in locations with strong seasonal variability and low in locations of weak seasonality. Vertically integrated respiration is weakly, yet significantly, correlated with remote observations of chlorophyll, net primary production, and planktonic community size structure. These correlations suggest that regimes of high net primary production and large phytoplankton fuel elevated respiration at depth. Several regions of float-based observations intersect with sites of other detailed observations (e.g., Hawaii and Sargasso Sea), which allows us to compare our results to independent studies. We find that there is good agreement among export production estimates at highly seasonal locations, and that float-based observations may be biased low at weakly seasonal locations. We posit that the reason for the low-latitude discrepancy is the relative steady state of oxygen concentration caused by weak seasonality and shallow wintertime mixed layer depths.

1. Introduction

The oceans are an important part of the global carbon cycle and act as a significant sink to atmospheric CO_2 [*Sarmiento and Gruber*, 2002; *Sabine et al.*, 2004] as planktonic communities transform carbon between organic and inorganic forms, and physical circulation acts to redistribute carbon inventory [*Hansell and Carlson*, 1998]. Remote sensing has been used since the 1970s to characterize the net primary production (*NPP*) at the surface of the ocean [*Hovis et al.*, 1980; *Platt and Sathyendranath*, 1988; *Platt et al.*, 1991]. The satellite observations have revealed that marine phytoplankton comprise approximately half of NPP globally [*Field et al.*, 1998].

Ultimately, a fraction of the organic matter formed at the surface sinks beneath the observational range of satellites (the first few tens of meters [*Gordon and McCluney*, 1975]), with the potential to undergo long-term sequestration [*Eppley and Peterson*, 1979]. This process has inefficiencies. As organic matter sinks from the surface, it is consumed by heterotrophs, and a large fraction is converted back to inorganic carbon (remineralized) via respiration before it reaches the abyssal ocean. *Martin et al.* [1987] characterized this depth-dependent carbon flux, and formulated the well-known Martin curve, a power function that describes the decrease in carbon flux with increasing depth.

There are many factors that influence the fraction of NPP that eventually escapes the euphotic zone, a ratio referred to as the *f* ratio. Models, verified by in situ data, indicate that the *f* ratio is affected by temperature (and latitude)-dependent growth rates [*Laws et al.*, 2000]. Planktonic community size structure is an important control on carbon export efficiency [*Henson et al.*, 2012; *Michaels and Silver*, 1988], as particle size distribution affects sinking rate. Larger particulate matter generally sinks faster (Stokes' law) and is exported from the euphotic zone more readily. Several studies have parameterized community structure based on remote chlorophyll and backscatter observations [*Kostadinov et al.*, 2009; *Hirata et al.*, 2011], which we later employ in comparison to our observations. Particulate matter can also aggregate during blooms, enhancing export [*Martin et al.*, 2011].

In recent years autonomous profiling floats have been used to characterize net community production (NCP), defined as NPP minus heterotrophic respiration. *Riser and Johnson* [2008] used data from two such floats in the subtropical Pacific that observed oxygen accumulation in the shallow oxygen maximum (<100 dbar) and determined that the elevated oxygen concentration was due to autotrophic production outpacing

respiration (positive NCP). *Martz et al.* [2008] used 18 floats with dissolved oxygen sensors to characterize the vertical structure of NCP (with an emphasis on 50 to 200 dbar) in the subpolar South Pacific and observed that remineralization exhibited a decrease with depth consistent with the Martin curve. Since 2008 (year of publication of the aforementioned Martz et al. and Riser and Johnson studies), the global coverage of profiling floats equipped with dissolved oxygen sensors has greatly expanded. The present work utilizes this increase in data volume to investigate the regional variability of ocean metabolism and carbon cycling.

Our aim is to estimate net respiration, referred to here as R, of heterotrophic communities below the mixed layer. R is not exactly equivalent to the carbon exported from the euphotic zone to the abyssal ocean, but rather an inefficiency in this transfer as the remineralized carbon can be ventilated back into the atmosphere by the annual formation of the deep wintertime mixed layer. Consequently, it is an important control on the fraction of NPP that is ultimately sequestered into the deep ocean for decades or longer. In fact, most of the export flux leaving the upper ocean is remineralized before it reaches the deep ocean [*Buesseler et al.*, 2007; *Henson et al.*, 2012]. Therefore, although we have no direct observations of carbon export, we can ascertain reasonable constraints on carbon flux out of the upper ~100 m and on export efficiency. We expect that R will be larger in regions of greater surface productivity, so we also make use of remote observations of surface production to identify possible correlations.

2. Methods

2.1. Float Data

We use data from 112 profiling floats equipped with Aanderaa Optode sensors (fabricated at the University of Washington; http://runt.ocean.washington.edu/o2/) to characterize submixed layer oxygen evolution. We avoid analysis in the mixed layer because, while the Optode sensors are stable over time (addressed further in section 2.2), there is a large factory calibration bias [*Gruber et al.*, 2007]. The bias of approximately 10–40 μmol kg^{-1} leads to prohibitively high error in air-sea gas exchange calculations. *Takeshita et al.* [2013] introduced a method using climatology to calibrate Optodes to ~3% error, and Robert Drucker of the University of Washington (unpublished data, 2015) has used a similar method that may reduce error to about 3 μmol kg^{-1} (~1%). Even with these improvements, a 3 μmol kg^{-1} error is still only sufficient to be confident in the sign of the air-sea gas exchange in most regions and leads to very large errors in mixed layer NCP estimates. Newer floats sample atmospheric oxygen, which allows calibration accurate enough to characterize NCP in the mixed layer [*Bushinsky and Emerson*, 2013]. However, the floats with this ability are currently limited in both number and breadth of spatial coverage.

Our estimates of R are more reliable if analysis is limited to depths below the mixed layer, where tracers are isolated from direct surface forcing. Here the temporal evolution of oxygen is more indicative of biological processes, and constraining our analysis to below the mixed layer takes advantage of the strength of the Optodes (precision and temporal stability) and eliminates the weaknesses (calibration bias) by focusing on the time rate of change of oxygen.

2.2. Calculating Net Respiration

In the methods used here, the float-based oxygen data are linearly interpolated to a pressure grid spaced by 10 dbar from the surface to 2000 dbar and a temporal grid spaced by 5 days, beginning at the first profile of a float and ending at the last. The choice of the pressure grid is designed to roughly reflect the oxygen sampling scheme of the floats in the upper ocean, while the temporal grid represents the floats' nominal 5 to 10 day cycle. The interpolated data are broken into temporal segments that span approximately 1 year, starting at one winter's maximum mixed layer depth and ending at the maximum mixed layer of the following year. This constitutes one float year of data. We use a density threshold of 0.125 kg m^{-3} or temperature threshold of 0.5°C, whichever is reached first, to estimate mixed layer depth [e.g., *Monterey and Levitus*, 1997].

As mentioned previously, we use the temporal evolution of oxygen to characterize biological influences on oxygen concentration. Autotrophic and heterotrophic processes are not the only factors that alter oxygen, however, as physical mechanisms also play a role, such that

$$\frac{d[O_2]}{dt} = 1.45 \times \mathrm{NCP} - \vec{u} \cdot \nabla[O_2] + \nabla \cdot (\kappa \nabla[O_2]) \quad (1)$$

where $\vec{u}$ is the three-dimensional velocity vector, and κ is the turbulent diffusivity tensor. We scale NCP by the Redfield ratio (1.45 O_2:1 C) to convert between organic carbon and O_2 [*Anderson and Sarmiento*, 1994].

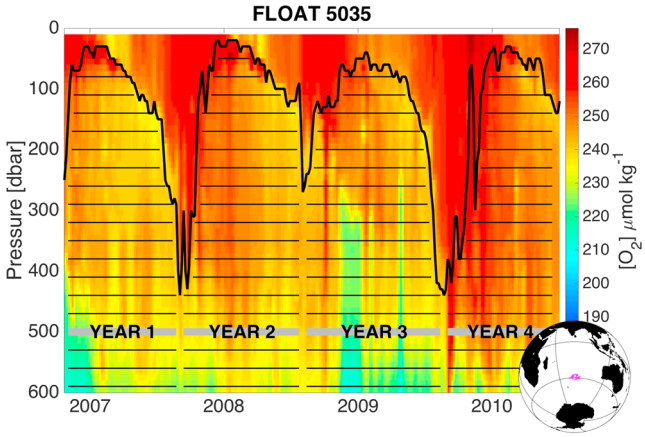

Figure 1. An example of oxygen evolution in the upper 600 m for UW float 5035 (World Meteorological Organization 1900722), located in the southern Indian Ocean. Thick black line: mixed layer depth. Horizontal black lines: time periods and depths for which the time rate of change of oxygen is calculated (for visual clarity, not every pressure level used is shown here). Small globe: the profile locations of float 5035 from 2007 to 2010 (magenta dots).

Surface flux terms are neglected because our analysis is constrained to beneath the mixed layer and 70 dbar (whichever is greater). We choose to omit data from the mixed layer for reasons outlined in section 2.1. The 70 dbar threshold is chosen because it is roughly at the compensation depth [*Najjar and Keeling*, 1997] (50–100 m), where respiration begins to outpace photosynthesis. We make the assumption that floats are equally likely to drift through positive and negative oxygen gradients, and given a large enough sample size, oxygen variability caused by water mass changes ($\vec{u} \cdot \nabla[O_2]$ and $\nabla \cdot (\kappa[O_2])$) tends to offset. We also assume that vertical diffusion is small [*Ledwell et al.*, 1993] and will play a minor role in oxygen evolution. Therefore, we use the simplification that oxygen evolution is dependent on NCP alone (revisited in section 4). Since our analysis is constrained to depths where it is common for respiration to outpace photosynthesis, we frame our results in terms of net respiration, R (where $R = -1 \times \mathrm{NCP}$), such that

$$R = -\frac{1}{1.45} \times \frac{\mathrm{d}[O_2]}{\mathrm{d}t} \tag{2}$$

Here positive R represents conditions of net destruction of organic matter via respiration. To determine R for a given float year, we first use least squares linear regression to find the best fit to the temporal evolution of oxygen concentration along isobars (Figure 1). The annual time rate of change of oxygen ($\mathrm{d}[O_2]/\mathrm{dt}$) is defined as the slope of this linear regression (Figure 2). In contrast to the constant temporal bounds used by *Martz et al.* [2008] (December to April), we calculate the respiration using the entire time that an isobar is below the mixed layer (see horizontal lines in Figure 1), so long as there are at least 100 uninterupted days. This variable temporal domain allows us to utilize the greatest possible number of available measurements.

Attempts to analyze oxygen trends on subannual timescales (e.g., months or seasons) did not reveal any obvious differences in the time rate of change of oxygen, unlike the signals with an annual period observed by *Najjar and Keeling* [1997]. We calculate annual respiration rates (in μmol C kg^{-1} yr^{-1}) from segments that are often less than 1 year and thus may expect some bias arising from extrapolation. However, due to the relative temporal consistency we observe in $\mathrm{d}[O_2]/\mathrm{dt}$, and because the temporal segments used often constitute a large fraction of the float year, we assume that these biases will be small.

This method yields vertical profiles of $\mathrm{d}[O]_2/\mathrm{dt}$ for each float year for all floats used in this study. Although the analysis presented here uses pressure surfaces as the vertical coordinate, our results are not highly sensitive to the choice of a pressure or density coordinate system, likely because isopycnal depth is not highly variable along the path of most floats.

We make the idealization that Optode sensors are stable in time, and $\mathrm{d}[O]_2/\mathrm{dt}$ is not influenced by instrument drift. Naturally, there is some degree of instrument drift, but the effects are presumed minor. Optodes have been found to drift ~0.3% per year [*Bushinsky et al.*, 2016], which will typically correspond to 1 μmol O_2 kg^{-1} yr^{-1} or less. We often see temporal O_2 changes of 10–20 μmol kg^{-1} yr^{-1} (Figure 2), so a drift on the order of 0.3% will not adversely affect our findings or interpretations.

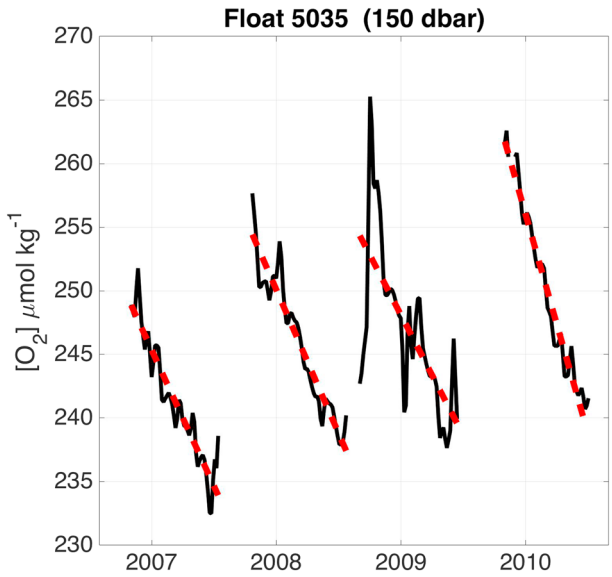

Figure 2. Solid black: oxygen concentration from UW float 5035 at 150 dbar (only when below the mixed layer). Dashed red: linear regression to each float year. The slope of this line is assumed to be the net oxygen consumption rate (or production if slope is positive).

Grouping float years by region allows us to diagnose both the variability and ensemble average of $d[O]_2/dt$ in areas with an abundance of floats equipped with Optodes (see example in Figure 3). Before calculating the ensemble mean, we visually inspect the data and remove float years in which sensors malfunctioned or the float obviously crossed a strong front (e.g., crossing the Gulf Stream in the Sargasso Sea), as these events can introduce extraordinarily strong oxygen signals that do not correspond to any biological processes. Regional results (Figure 4) are discussed in section 3.1.

We also calculate the depth-integrated respiration, R_{sub} for each float year, such that

$$R_{sub} = \int_{70dbar}^{P_{max}} R(p)dp \tag{3}$$

where $R(p)$ is the pressure-dependent net respiration (R). As mentioned previously, we choose 70 dbar as the lower limit on pressure because it roughly coincides with the compensation depth. The upper limit

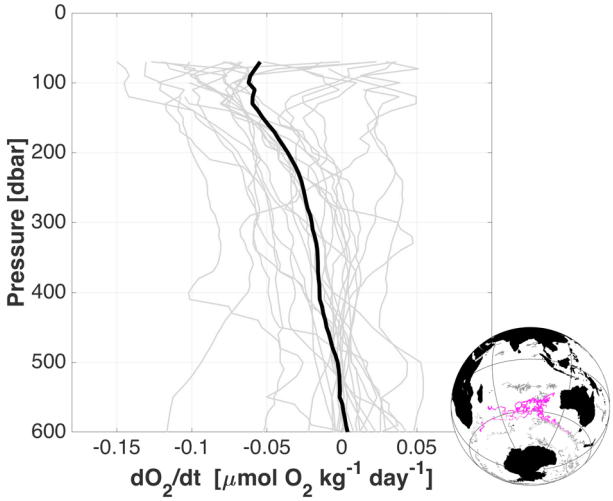

Figure 3. Twenty-five vertical profiles of oxygen time rate of change calculated from each float year in the southern Indian region. The thick black line is the ensemble mean. Small globe shows the float profiles used (magenta) and unused (grey) in main panel.

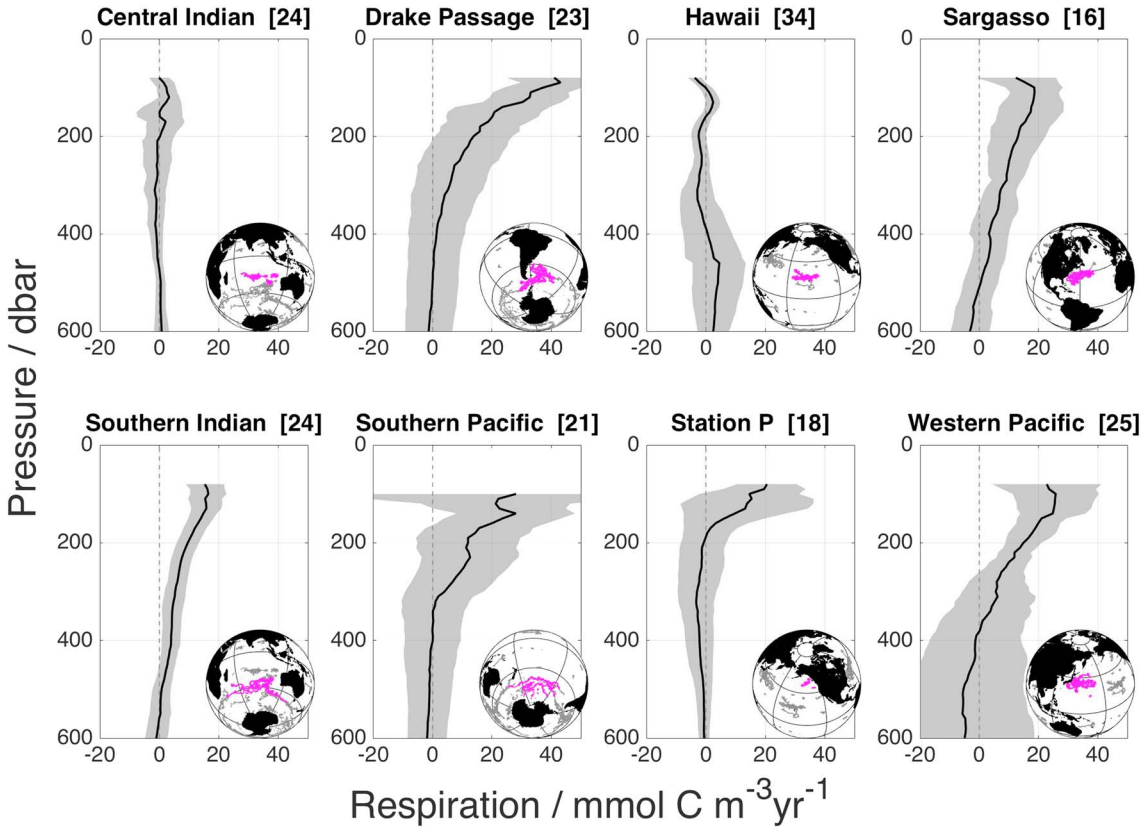

Figure 4. Depth profiles of net respiration rate (R) determined from floats with Optode oxygen sensors. The thick black line is the mean profile calculated from the ensemble of float years in the given region, while the shaded region is the 95% confidence interval (assuming Gaussian distribution). The bracketed number is the number of float years used in each region. The small globe shows the locations of profiles used (magenta) and unused (grey) in regional composite.

of integration, P_{max}, varies regionally and is the point at which the mean respiration rates reach zero (e.g., ~500 dbar in Figure 3). We do not integrate beyond P_{max} because $R(p)$ is generally indistinguishable from zero at pressures greater than P_{max}. Similar to $R(p)$, R_{sub} is an extrapolation to an annual depth-integrated respiration rate based on partial temporal coverage of the float year.

2.3. Correlation With Surface Variables

The depth profiles of R (Figure 4) suggest a high degree of spatial variability in subsurface respiration. Next, we aim to examine several surface variables and how they may be related to subsurface respiration. The surface data sets examined are as follows: (1) chlorophyll *a*, hereafter *Chl* (satellite observations of chlorophyll concentration from Moderate-resolution Imaging Spectroradiometer [*Esaias et al.*, 1998]); (2) community structure, hereafter ξ [*Kostadinov et al.*, 2009] (based on satellite observations of ocean color. ξ describes the particle size distribution; lower values represent communities with larger particles, and higher values represent communities with smaller particles); (3) vertically generalized production model, hereafter VGPM; [*Behrenfeld and Falkowski*, 1997] (a parameterized estimate of NPP, primarily based on remote observations of chlorophyll); and (4) carbon-based production model, hereafter CbPM [*Westberry et al.*, 2008] (Similar to VGPM, but this parameterization of NPP also uses remote observations of backscatter to estimate planktonic carbon content.)

For each float year, R_{sub} is compared with the surface variables over the same time period (Figure 5). To make these comparisons, we average the surface variables both temporally and spatially. We take the mean of all surface data within 100 km of the float at each monthly time bin and then use the monthly means to calculate an average over the entire float year (and convert to an annual rate, in the case of the VGPM and CbPM NPP data). Using 100 km as a threshold effectively creates an area of averaging that is 200 km in diameter. This is slightly larger than the typical mesoscale length scale (~100 km), which smoothes some of the variability caused by the mesoscale field without being so large that it includes environments far from the domain of the float.

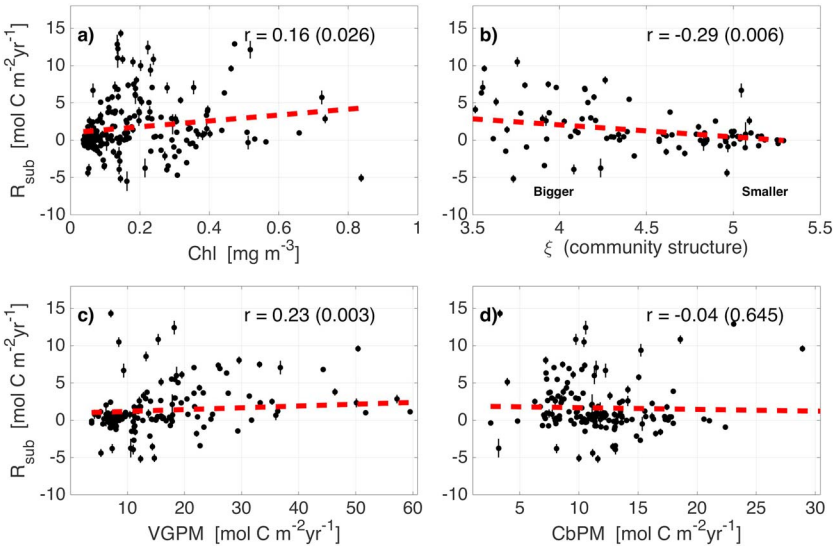

Figure 5. Correlation between surface variables and the subsurface respiration, R_{sub}. In each panel the black points show data that are used for determining the correlation coefficient, r (with the corresponding p value in parentheses). Vertical error bars are established by summing (in quadrature) the error from the d[O_2]/dt estimates in the pressure range used in equation (3) and scaling by the Redfield ratio to convert from oxygen to organic carbon. The red dashed line is the linear regression to the black points.

We remove the lower and upper 1% of both remote observations and float data before calculating correlation coefficients (treating these observations as outliers).

2.4. Export Production and Efficiency

To estimate the export efficiency (f ratio) in the different regions examined in this study, we couple our in situ observations of R_{sub} with satellite measurements of NPP. We use the VGPM estimate of NPP since it is better correlated to our respiration data than the CbPM model (Figure 5). We use the depth-integrated respiration, R_{sub}, as a proxy for the export flux of organic matter at 70 m. This estimate of export flux is likely to be a lower bound of the true carbon flux (i.e., $R_{sub} \leq$ export), because almost certainly some (small) fraction of the exported organic matter will pass below P_{max} [*Buesseler et al.*, 2007] before being remineralized. The f ratio is defined as

$$f - \text{ratio} = \frac{\text{NCP}}{\text{NPP}} \tag{4}$$

where we treat NCP as equivalent to the export of organic matter at 70 m (assuming steady state). Our float-based estimate of the export efficiency, f_F, is thus defined as

$$f_F = \frac{R_{sub}}{\text{NPP}_{vgpm}} \tag{5}$$

where R_{sub} is defined as in equation (3), and NPP_{vgpm} is the monthly VGPM parameterization of remote observations [*Behrenfeld and Falkowski*, 1997]. Each float year yields a single estimate of f_F by combining the measured R_{sub} and mean NPP_{vgpm} over that time span (NPP_{vgpm} is averaged in the same manner as in section 2.3). Since we assume that R_{sub} is a lower bound for the carbon exported out of the euphotic zone, it follows that f_F is a lower bound on the true f ratio.

To construct a standard by which to compare our observations, we also calculate the f ratio using two independent parameterizations. *Dunne et al.* [2005] used temperature, NPP, and the euphotic zone depth (Z_{eu}) to parameterize the f ratio, hereafter f_D, as

$$f_D = -0.0101°\text{C}^{-1} \times T + 0.0683 \times \ln(\text{NPP}/Z_{eu}) + 0.419. \tag{6}$$

Here we set Z_{eu} as a constant (100 m), use NPP_{vgpm} as the primary production term, and take T to be the monthly average of the corresponding uppermost temperature measurements from the float profiles (usually ~5 dbar). *Henson et al.* [2011] used *Laws et al.* [2000] observations of temperature and export efficiency to formulate a temperature-only based parameterization of the f ratio, hereafter f_L, as

$$f_L = 0.62 - (0.02 \times T) \tag{7}$$

where we define T as in equation (6). We use the monthly estimates of NPP_{vgpm} and T to calculate f_L and f_D for each month.

As with the f ratio, we would like to also have a benchmark by which to compare the values of R_{sub} (our proxy for export). We calculate two estimates of the export production, E_D [*Dunne et al.*, 2005] and E_L [*Laws et al.*, 2000]:

$$E_D = NPP_{vgpm} \times f_D \tag{8}$$

$$E_L = NPP_{vgpm} \times f_L \tag{9}$$

where we use the monthly estimates of NPP_{vgpm}, f_D, and f_L. Results of calculations using equations (5)–(9) are presented in section 3.3.

2.5. Comments on Methods

The simplifications leading from equation (1) to equation (2) are necessary due to the uncertainties in the advective and diffusive terms. In most of the regions we examine, this is a reasonable approximation given that the advective-diffusive terms are expected to be small and we see robust signals in $d[O_2]/dt$. However, in weakly seasonal locations (e.g., low latitude), where the magnitude of the advective-diffusive terms are comparable to $d[O_2]/dt$, equation (2) may be insufficient to determine the respiration. Weakly seasonal locations generally have little difference between summertime and wintertime mixed layer depths, and biological production tends to be relatively consistent with time [*Behrenfeld and Falkowski*, 1997]. These factors lead to a relatively steady oxygen concentration ($d[O_2]/dt \sim 0$), and using equation (2) would suggest negligible respiration; however, in these regions the advective-diffusive terms are actually offsetting respiration. In contrast, regions with higher seasonality in physical and biological processes (e.g., high latitude) show strong signals in $d[O_2]/dt$ and equation (2) is likely a reasonable assumption. The performance of our methods will be further evaluated in section 4.3 where we contrast our observations to past results.

3. Results

3.1. Regional Respiration Profiles

We estimate R in eight distinct regions globally, ranging from the North Pacific to the Southern Ocean (Figure 4). All locations have at least 16 float years of data (with a maximum of 34 at Hawaii), providing a reasonable statistical sample size by which to evaluate the ensemble behavior. The 95% confidence intervals (assuming Gaussian distribution) show that mean vertical profiles of R are generally distinct from zero in the upper ocean. The vertical structure and magnitude of R is significantly variable across different regions. High latitudes and locations where the mixed layer undergoes drastic seasonal changes tend to have much stronger respiration signals. Conversely, some subtropical sites (Hawaii and central Indian Ocean) exhibit negligible respiration. In section 4 we discuss these results and their significance further.

3.2. Correlations Between R_{sub} and Surface Variables

There are weak, but significant (p value < 0.05), correlations between R_{sub} and the remote estimates of Chl and VGPM, while R_{sub} is significantly anticorrelated with ξ and not correlated with CbPM (Figure 5).

As Chl and VGPM rise, so does R_{sub} which suggests, as one would expect, that as more organic matter is created at the surface, more sinks below the euphotic zone, resulting in greater heterotrophic respiration and remineralization. The negative correlation between ξ and R_{sub} may be a result of larger phytoplankton sinking out of the euphotic zone more readily (less nutrient recycling), fueling greater respiration at depth.

It is somewhat difficult to disentangle these results, as all the surface variables are highly correlated with one another since they share the same underlying data (remote observations of color and backscatter), but our results suggest that more productive regions fuel greater respiration at depth. There could be significant noise

Table 1. Regional Estimates of R_{sub} (Equation (3); a Proxy for Export) and f Ratio (Equation (5)) From Profiling Floats With Mean and 95% CI[a]

Region	f ratio	Export (mol C m^{-2} yr^{-1})	NCP (mol C m^{-2} yr^{-1})
Central Indian	0.02 ± 0.08	0.1 ± 0.5	-
Drake Passage	0.68 ± 0.55	4.4 ± 2.9	-
Hawaii	0.00 ± 0.03	-0.1 ± 0.2	2.5 ± 0.7[b]
Sargasso	0.34 ± 0.16	3.9 ± 2.3	3.8 ± 1.2[c]
Southern Indian	0.36 ± 0.13	3.8 ± 1.1	-
Southern Pacific	0.47 ± 0.77	3.2 ± 3.2	-
Station P	0.19 ± 0.22	1.3 ± 1.5	2.3 ± 0.6[b]
Western Pacific	0.42 ± 0.28	3.8 ± 1.8	2.9 ± 0.2[c]

[a]The rightmost column shows results from previous publications, where available. Here NCP is expected to be roughly similar to export.
[b]Annual Net Community Production. *Emerson* [2014].
[c]Total NCP between winter and September. *Midorikawa et al.* [2002].

introduced by errors in yearly estimates of R_{sub}. Remote observations are well known to have significant error [*Hooker and McClain*, 2000]. Thus, there may be a substantial amount of variance in R_{sub} left unexplained by surface processes, as there is only a weak correlation. This underscores the importance of collecting in situ subsurface measurements, as satellite observations only offer a narrow window into the full complexities of carbon cycling.

3.3. Export and Export Efficiency

Our regional calculations of export flux (equation (3)) and the f ratio (equation (5)) are summarized in Table 1. It bears repeating that we expect these estimates to be lower bounds of the f ratio and export production, as elucidated in section 2.4. The float observations reveal significant variability in export efficiency (Figure 6, yellow bars) and export (Figure 7, yellow bars) across the World Ocean. At midlatitude to high latitude, the integrated respiration (our proxy for export) and f ratio values are generally higher, while in some subtropical regions (Hawaii, and central Indian Ocean) we find essentially no respiration export below the compensation depth (assumed 70 m). We also contrast these observations with parameterizations of the f ratio (f_D, equation (6) and f_L, equation (7)) and export (E_D, equation (8) and E_L, equation (9)), shown in Figures 6 and 7, respectively.

The parameterizations display the same trend as our observations; values of export and export efficiency are generally higher at high latitude, while low nearer the tropics. There are several regions of significant difference, however. For example, the Sargasso Sea float observations of the f ratio and export are higher than the parameterizations. This disagreement could arise from several issues.

As stated in section 2.4, we expect our float-based estimates to be lower bounds of the true values of the f ratio and export. This suggests that E_D and/or E_L are too low in regions where they fall significantly short of R_{sub}, as in the Sargasso Sea (Figure 7). The difference here could arise from local inaccuracies in equations (6) and (7) (which are formulated to fit global trends) or from errors in satellite measurements of NPP, which can be as large as 35% [*Hooker and McClain*, 2000]. In several regions (e.g., Hawaii) float-based observations are significantly lower than parameterizations, and we explore this further in section 4.3.

4. Discussion

4.1. Comparison to Previous Work

Several of the regions in the work (Hawaii, Sargasso Sea, Station P, and Western Pacific) coincide with areas that are very well studied and have many estimates of surface NCP. Again, we assume that on annual timescales the upper ocean is at steady state, and the estimates of NCP from these studies are approximately equal to the export flux, which in turn is largely remineralized in the upper ocean [*Martin et al.*, 1987; *Buesseler et al.*, 2007]. We do not expect NCP at the surface to exactly match our observations of R_{sub}; however, they are likely similar in scale.

Our estimates of R_{sub} in the Sargasso and Western Pacific regions are in general agreement with the observations of surface NCP by other studies (see Table 1). Observations of tracer-based apparent oxygen utilization

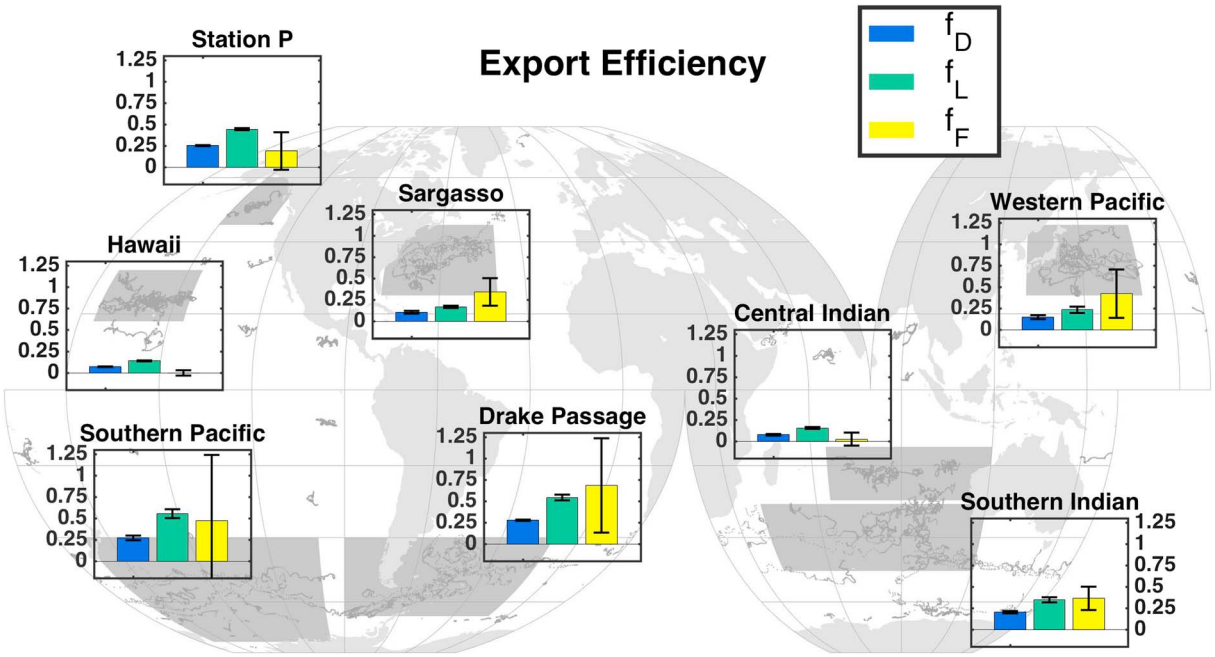

Figure 6. Regional estimates of the *f* ratio. Dark grey dots are profile locations of floats used in this study. Shaded grey regions are the spatial boundaries used to delineate regions, and accompanying small bar plots show the regional *f* ratio calculated by several means. Yellow: estimates of f_F derived from float and satellite observations. Blue and green: parameterizations of export efficiency (f_D and f_L). Error bars on estimates are 95% confidence interval assuming Gaussian distribution (see Figure 4 for number of float years in each region.)

rates (AOUR) in the Sargasso Sea also allow us to make a more direct comparison. *Stanley et al.* [2012] found AOUR to be 3.1 ± 0.5 mol O_2 m^{-2} yr^{-1} in the upper 500 m, which is about half of what we estimate from float observations. This difference may be at least partially attributable to spatial variability, as the floats are not tightly clustered around the site examined by *Stanley et al.* [2012] and we do observe spatial gradients in R_{sub} in the Sargasso Sea. In contrast to past results, our observations at Station P are somewhat low and very low at Hawaii [*Emerson*, 2014]. In order to diagnose the performance of our methods (oxygen evolution on profiling floats), we further examine what may cause such discrepancies.

4.2. Comparison to HOT and BATS

To augment our analysis, we also compute *R* at Hawaii Ocean Time Series (HOT) [*Karl and Lukas*, 1996] and Bermuda Atlantic Time Series (BATS) [*Michaels and Knap*, 1996] using those sites' oxygen concentration time series and utilizing the same analysis used for float oxygen data (section 2.2). The temporal resolution (approximately monthly) is not as fine as float cycles, but this should not negatively impact our results. The vertical structure of the net respiration profile based on BATS data is similar to the nearby float data (Figure 8, left), with a moderate difference in magnitude. Examination of individual float year data suggests that this discrepancy in magnitude is due to spatial variability, where float data collected closer to the BATS site show the most similarity. The HOT-based net respiration estimates and Hawaiian float data (Figure 8, right) both suggest that *R* is quite weak in the region. It is encouraging that *R* calculated from multidecadal time series generally corroborate the float-based measurements. However, the method of using oxygen evolution as a proxy for biological metabolism (equation (2)) must be scrutinized.

4.3. Method Examination

The large difference between float measured R_{sub} and past observations of upper ocean NCP at HOT may have several different interpretations. First, it could indicate high transfer efficiency, where a very large fraction of the new production at the surface makes its way to the deep ocean, bypassing remineralization. Second, it could suggest the magnitude of biological production in the region is substationally different than has previously been assumed. Third, it could reveal that our methods have shortcomings, and under certain conditions we are unable to adequately capture the submixed layer respiration.

Carbon flux usually exhibits a strong decrease with depth [*Martin et al.*, 1987], so it would be unusual for such a large fraction (well over 50%) of carbon to escape to great depth without being remineralized. We are also

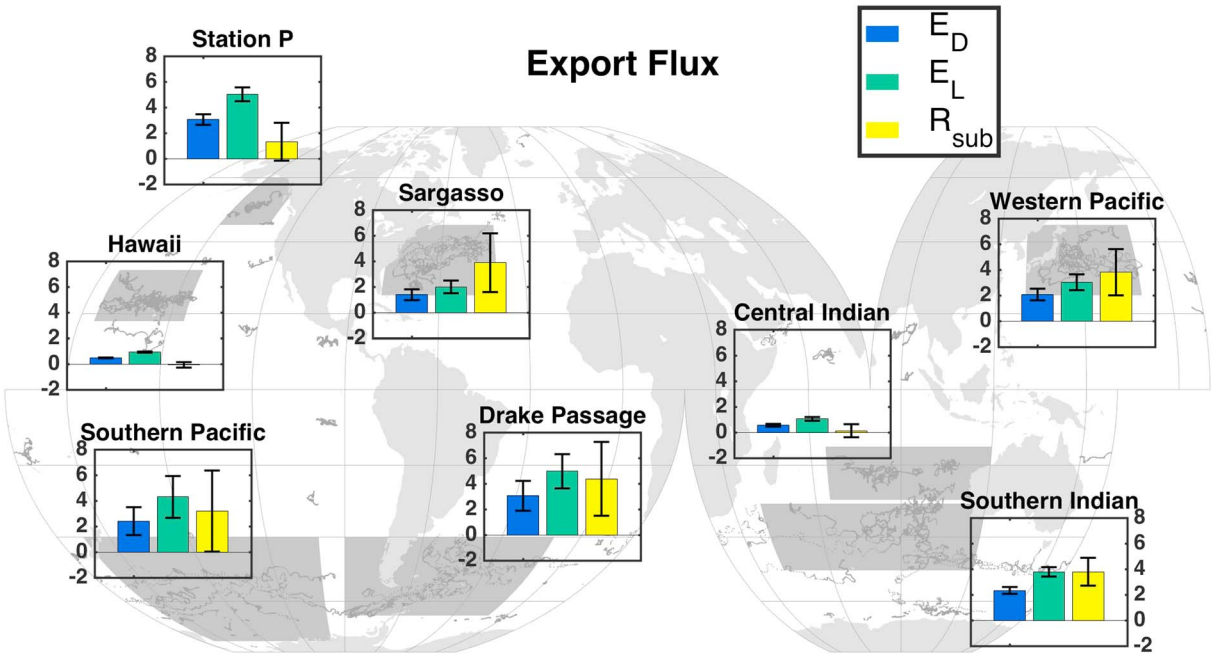

Figure 7. Identical to Figure 6 but for carbon export. E_D and E_L are based on parameterizations, and R_{sub} is a lower bound of export estimated from float-observed respiration. Units are in mol C m^{-2} yr^{-1}.

hesitant to claim that the float-based estimates of respiration are representative of the Hawaiian region, as we expect the depth-integrated respiration to be of similar scale to past estimates of euphotic zone NCP. *Emerson* [2014] compiled numerous independent studies and estimated NCP to be 2.5 ± 0.7 mol C m^{-2} yr^{-1} at HOT, while we observe essentially no statistically significant respiration below the euphotic zone. This leads to the examination of the third reason for the potential discrepancy.

Thus far, we have employed equation (2) with the assumption that (at least for ensemble averages) advective and diffusive terms can be neglected. However, equation (1) demonstrates that there can be significant respiration without a corresponding change in oxygen concentration (e.g., $d[O_2]/dt = 0$), so long as there are

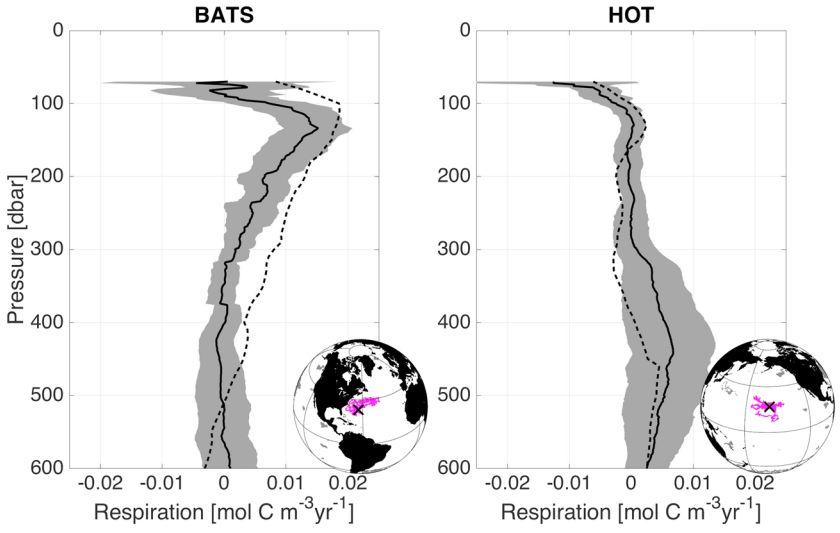

Figure 8. The net respiration profile calculated from oxygen time series at (right) HOT and (left) BATS. The solid black line is the mean respiration, and the shaded grey is the 95% confidence interval. The dashed line is the mean of the corresponding float data (identical to Figure 4). The small globes show the locations of profiles used (magenta) and unused (grey) in the regional mean, as well as the HOT/BATS sites (black cross).

balancing advective-diffusive contributions. Consequently, our low values obtained at HOT could be biased by physical interference.

In order to investigate the potential effect of lateral advection on our observations (i.e., the horizontal terms in $\vec{u} \cdot \nabla O_2$), we utilize World Ocean Atlas (WOA) oxygen climatology [*Garcia et al.*, 2010]. Here we assume that oxygen concentrations are constant in time and vary only along the float path. We linearly interpolate the WOA oxygen to the floats' position, thereby creating synthetic oxygen time series determined solely by float drift. We then applied equation (2) to the WOA-based oxygen time series to examine potential bias from float advection. Based off of this simple analysis, we find that none of the regions examined in Figure 4 have a contribution from horizontal float advection that is statistically different from zero. This is not to suggest that advection plays no role in biasing our measurements, but it may not be the primary factor in the discrepancy between float observations and other methods.

In addition to lateral float advection, vertical pumping and diffusion could account for the disagreement between float data and other studies. Hawaii is a region of general downwelling caused by the dominant local wind stress curl [*Risien and Chelton*, 2008] and coupled with the vertical structure of oxygen in the region; it could play a role in replenishing oxygen and obscuring our observations of *R*. Similarly, vertical diffusion could act to oxygenate the submixed layer, creating a net downward flux of oxygen and counteracting the effects of respiration.

There are a number of large uncertainties associated with the physical terms in equation (1) that prevent us from accurately quantifying the physical impact on oxygen. First, diffusion terms are uncertain and difficult to accurately constrain. Second, we do not have reliable estimates of velocities associated with Ekman pumping. Last, our aforementioned analysis of lateral advection is based on climatology that cannot replicate the true complexity of the oxygen field traversed by the floats. When oxygen is at steady state, respiration is essentially the residual of the physical terms in equation (1). Without a strong respiration signal even small uncertainties in the physical terms compound and make it impossible to deduce respiration.

However, in locations well sampled by other studies (Hawaii, Sargasso Sea, Western Pacific, and Station P), we can arrive at some qualitative observations on the effectiveness of this method. In regions where there is a deep wintertime mixed layer ($\geq$ 200 m) and a high degree of ventilation (Sargasso Sea and Western Pacific) there is good agreement with previous estimates. Regions of relatively shallow wintertime mixed layers ($\sim$100 m) do not corroborate past results. We find R_{sub} to be negligible to small at both Hawaii and Station P, while we expect values to be approximately 2 to 4 mol C m^{-2} yr^{-1} in these regions [*Sonnerup et al.*, 2013; *Emerson*, 2014]. We therefore suggest that attempts to diagnose net respiration and remineralization solely based on temporal oxygen evolution will perform reasonably well in regions where the mixed layer undergoes large seasonal change and fare poorly where ventilation is weakly seasonal.

5. Conclusions

There are several central results from this study. The vertical structure and overall magnitude of net respiration are highly variable across different global regions. Generally, we estimate that export and export efficiency are greater at higher latitudes, which corroborate past studies [*Laws et al.*, 2000; *Dunne et al.*, 2005; *Henson et al.*, 2012]. However, our observations may be biased low at low latitude and regions with weakly seasonal mixed layer depth and shallow seasonal pycnoclines.

The float-based estimates of export and export efficiency that we expect are reliable in Drake Passage (export = 4.4 $\pm$ 2.9 mol C m^{-2} yr^{-1}; *f* ratio = 0.68 $\pm$ 0.55), Sargasso Sea (3.9 $\pm$ 2.3, 0.34 $\pm$ 0.16), Southern Indian Ocean (3.8 $\pm$ 1.1; 0.36 $\pm$ 0.13), and Western Pacific (3.8 $\pm$ 1.8; 0.42 $\pm$ 0.28).

There is weak, yet significant, correlation between subsurface respiration (R_{sub}) and surface variables, where greater production and larger community structure tend to accompany greater respiration at depth. The weak correlation could be partially caused by variability in respiration rates caused by physical advection or large errors in satellite-derived data products. However, it highlights the importance of field observations in determining net community production and respiration.

Ultimately, as the population of profiling floats equipped with dissolved oxygen sensors grows, so too will our ability to observe net respiration and remineralization in the ocean. Greater sample sizes will allow more precise regional characterizations, and a greater breadth of spatial coverage will enable further exploration of

important aspects of the global carbon cycle. Although this method has shortcomings, mostly at low latitudes, the majority of export production (and hence remineralization) occurs at midlatitude to high latitude [*Henson et al.*, 2011], suggesting profiling floats equipped with appropriate sensors can make valuable contributions to carbon cycling research.

Acknowledgments
This work was generously supported by University of Washington grant NA15OAR4320063 and grants OPP-1353177 and OPP-1429342 from the National Science Foundation. The float data presented here can be accessed at http://runt.ocean.washington.edu/o2/. All other data used are attributed in the references. The floats were all fabricated at the University of Washington from components purchased from Teledyne/Webb Research. We thank Dana Swift, Rick Rupan, and Greg Brusseau of the University of Washington for their superb skills in producing these high-quality instruments. We thank Steven Emerson for valuable discussions that substantially improved the content of the manuscript, as well as Shirley Leung for discussions on remote observations of community structure. We also thank two anonymous reviewers for comments that helped clarify and improve the manuscript.

References

Anderson, L. A., and J. L. Sarmiento (1994), Redfield ratios of remineralization determined by nutrient data analysis, *Global Biogeochem. Cycles*, *8*, 65–80.

Behrenfeld, M. J., and P. G. Falkowski (1997), Photosynthetic rates derived from satellite-based chlorophyll concentration, *Limnol. Oceanogr.*, *42*, 1–20.

Buesseler, K. O., et al. (2007), Revisiting carbon flux through the ocean's twilight zone, *Science*, *316*, 567–570.

Bushinsky, S. M., and S. Emerson (2013), A method for in-situ calibration of Aanderaa oxygen sensors on surface moorings, *Mar. Chem.*, *155*, 22–28, doi:10.1016/j.marchem.2013.05.001.

Bushinsky, S. M., S. R. Emerson, S. C. Riser, and D. D. Swift (2016), Accurate oxygen measurements on modified Argo floats using in situ air calibrations, *Limnol. Oceanogr. Methods*, doi:10.1002/lom3.10107.

Dunne, J. P., R. A. Armstrong, A. Gnanadesikan, and J. L. Sarmiento (2005), Empirical and mechanistic models for the particle export ratio, *Global Biogeochem. Cycles*, *19*, GB4026, doi:10.1029/2004GB002390.

Emerson, S. (2014), Annual net community production and the biological carbon flux in the ocean, *Global Biogeochem. Cycles*, *28*, 14–28, doi:10.1002/2013GB004680.

Eppley, R. W., and B. J. Peterson (1979), Particulate organic matter flux and planktonic new production in the deep ocean, *Nature*, *282*, 677–680.

Esaias, W. E., et al. (1998), An overview of MODIS capabilities for ocean science observations, *IEEE Trans. Geosci. Remote Sens.*, *36*(4), 1250–1265.

Field, C. B., M. J. Behrenfeld, J. T. Randerson, and P. Falkowski (1998), Primary production of the biosphere: Integrating terrestrial and oceanic components, *Science*, *281*, 237–240, doi:10.1126/science.281.5374.237.

Garcia, H., R. Locarnini, T. Boyer, J. Antonov, O. Baranova, M. Zweng, and D. Johnson (2010), *World Ocean Atlas 2009, Volume 3: Dissolved Oxygen, Apparent Oxygen Utilization, and Oxygen Saturation*, edited by S. Levitus, 344 pp., NOAA Atlas SESDIS 70, U.S. Gov. Print. Off., Washington, D. C.

Gordon, H. R., and W. R. McCluney (1975), Estimation of the depth of sunlight penetration in the sea for remote sensing, *Appl. Opt.*, *14*(2), 413–416.

Gruber, N., S. C. Doney, S. R. Emerson, D. Gilbert, T. Kobayashi, A. Körtzinger, G. C. Johnson, K. S. Johnson, S. C. Riser, and O. Ulloa (2007), The Argo-Oxygen Program, (White Paper), [Available at http://www-argo.ucsd.edu/o2_white_paper_web.pdf.]

Hansell, D. A., and C. A. Carlson (1998), Deep-ocean gradients in the concentration of dissolved organic carbon, *Nature*, *395*, 263–266.

Henson, S. A., R. Sanders, E. Madsen, P. J. Morris, F. Le Moigne, and G. D. Quartly (2011), A reduced estimate of the strength of the ocean's biological carbon pump, *Geophys. Res. Lett.*, *38*, L04606, doi:10.1029/2011GL046735.

Henson, S. A., R. Sanders, and E. Madsen (2012), Global patterns in efficiency of particulate organic carbon export and transfer to the deep ocean, *Global Biogeochemical Cycles*, *26*, GB1028, doi:10.1029/2011GB004099.

Hirata, T., et al. (2011), Synoptic relationships between surface Chlorophyll a and diagnostic pigments specific to phytoplankton functional types., *Biogeosciences*, *8*, 311–327, doi:10.5194/bg-8-311-2011.

Hooker, S. B., and C. R. McClain (2000), The calibration and validation of SeaWiFS data, *Prog. Oceanogr.*, *45*, 427–465.

Hovis, W. A., et al. (1980), Nimbus-7 Coastal Zone Color Scanner: System description and initial imagery, *Science*, *210*, 60–63.

Karl, D. M., and R. Lukas (1996), The Hawaii Ocean Time-series (HOT) program: Background, rationale and field implementation, *Deep Sea Rese., Part II*, *43*, 129–156, doi:10.1016/0967-0645(96)00005-7.

Kostadinov, T. S., D. A. Siegel, and S. Maritorena (2009), Retrieval of the particle size distribution from satellite ocean color observations, *J. Geophys. Res.*, *114*, C09015, doi:10.1029/2009JC005303.

Laws, E. A., P. G. Falkowski, W. O. Smith Jr., H. Ducklow, and J. J. McCarthy (2000), Temperature effects on export production in the open ocean, *Global Biogeochem. Cycles*, *14*(4), 1231–1246.

Ledwell, J., A. J. Watson, and C. S. Law (1993), Evidence for slow mixing across the pycnocline from an open-ocean tracer-release experiment, *Nature*, *364*, 701–703.

Martin, J. H., G. A. Knauer, D. M. Karl, and W. W. Broenkow (1987), VERTEX: Carbon cycling in the northeast Pacific, *Deep Sea Res., Part A*, *34*(2), 267–285.

Martin, P., R. S. Lampitt, M. Jane Perry, R. Sanders, C. Lee, and E. D'Asaro (2011), Export and mesopelagic particle flux during a North Atlantic spring diatom bloom, *Deep Sea Res., Part I*, *58*(4), 338–349, doi:10.1016/j.dsr.2011.01.006.

Martz, T. R., K. S. Johnson, and S. C. Riser (2008), Ocean metabolism observed with oxygen sensors on profiling floats in the South Pacific, *Limnol. Oceanogr.*, *53*(5–2), 2094–2111.

Michaels, A. F., and A. H. Knap (1996), Overview of the U.S. JGOFS Bermuda Atlantic time-series study and the hydrostation S program, *Deep Sea Res., Part II*, *43*(2–3), 157–198.

Michaels, A. F., and M. W. Silver (1988), Primary production, sinking fluxes and the microbial food web, *Deep Sea Res.*, *35*(4), 473–490.

Midorikawa, T., T. Umeda, N. Hiraishi, K. Ogawa, K. Nemoto, N. Kubo, and M. Ishii (2002), Estimation of seasonal net community production and air-sea CO_2 flux based on the carbon budget above the temperature minimum layer in the western subarctic North Pacific, *Deep Sea Res., Part I*, *49*, 339–362.

Monterey, G., and S. Levitus (1997), *Seasonal Variability of Mixed Layer Depth for the World Ocean, NOAA Atlas NESDIS 14*, Natl. Oceanic and Atmos. Admin., 100 pp., Silver Spring, Md.

Najjar, R. G., and R. F. Keeling (1997), Analysis of the mean annual cycle of the dissolved oxygen anomaly in the World Ocean, *J. Mar. Res.*, *55*, 117–151.

Platt, T., and S. Sathyendranath (1988), Oceanic remote primary production: Estimation by remote sensing at local and regional scales, *Science*, *241*, 1613–1620.

Platt, T., C. Caverhill, and S. Sathyendranath (1991), Basin-scale estimates of oceanic primary production by remote sensing: The North Atlantic, *J. Geophys. Res.*, *96*(C8), 15,147–15,159.

Riser, S. C., and K. S. Johnson (2008), Net production of oxygen in the subtropical ocean, *Nature*, *451*, 323–325.

Risien, C. M., and D. B. Chelton (2008), A global climatology of surface wind and wind stress fields from eight years of QuikSCAT scatterometer data, *J. Phys. Oceanogr.*, *38*, 2379–2413.
Sabine, C. L., et al. (2004), The oceanic sink for anthropogenic CO_2, *Science*, *305*, 367–371.
Sarmiento, J., and N. Gruber (2002), Sinks for anthropogenic carbon, *Phys. Today*, *55*, 30–36.
Sonnerup, R. E., S. Mecking, and J. L. Bullister (2013), Transit time distributions and oxygen utilization rates in the northeast Pacific Ocean from chlorofluorocarbons and sulfur hexafluoride, *Deep Sea Res.*, *1*(72), 61–71.
Stanley, R. H. R., S. C. Doney, W. J. Jenkins, and D. E. Lott III (2012), Apparent oxygen utilization rates calculated from tritium and helium-3 profiles at the Bermuda Atlantic Time-series Study site, *Biogeosciences*, *9*, 1969–1983.
Takeshita, Y., T. R. Martz, K. S. Johnson, J. N. Plant, D. Gilbert, S. C. Riser, C. Neill, and B. Tilbrook (2013), A climatology-based quality control procedure for profiling float oxygen data, *J. Geophys. Res. Oceans*, *118*, 5640–5650, doi:10.1002/jgrc.20399.
Westberry, T., M. J. Behrenfeld, D. A. Siegel, and E. Boss (2008), Carbon-based primary productivity modeling with vertically resolved photoacclimation, *Global Biogeochem. Cycles*, *22*, GB2024, doi:10.1029/2007GB003078.